Numerical Derivation of Dispersion Coefficients for Flow through Three-Dimensional Randomly Packed Beds of Monodisperse Spheres

Amir Jourak, J. Gunnar I. Hellström, and T. Staffan Lundström
Div. of Fluid and Experimental Mechanics, Luleå University of Technology, Luleå SE-971 87, Sweden

Vilnis Frishfelds
Faculty of Natural Sciences, Liepaja University, Liela iela 14, Liepaja LV-3401, Latvia

DOI 10.1002/aic.14284
Published online November 15, 2013 in Wiley Online Library (wileyonlinelibrary.com)

The longitudinal (D_L) and transverse (D_T) dispersion coefficients for flow through randomly packed beds of discrete monosized spherical particles are studied. The three-dimensional (3-D) porous-medium model consists of thousands of spherical particles that are divided into cells using Voronoi diagrams. The relationship between the variation of the dual stream function and the vorticity between neighboring particles is derived using Laurent series. The whole flow pattern at low particle Reynolds number is then obtained by minimization of the dissipation rate of energy with respect to the dual stream function. The D_L is obtained by fitting the resulting effluent curve to a 1-D solution of a continuous model. The D_T is obtained by fitting the numerical concentration profile to an approximate 2-D solution. The derived D_L and D_T values are in agreement with 3-D experimental data from the literature enabling a study of the effects of pore structure and porosity on D_L and D_T. © 2013 American Institute of Chemical Engineers *AIChE J*, 60: 749–761, 2014
Keywords: longitudinal dispersion, transverse dispersion, mass transfer, dual stream function, Voronoi diagrams, permeability

Introduction

Pore-scale flow and dispersion in porous media like in fixed beds of spheres has been modeled in different fields of engineering. One example is compact-bed filters that are used for on-site sanitation systems.[1–3] Modeling the flow through such packed beds in laboratory scale is important for aspects such as geometrical scale-up and optimization of operation parameters.[4] In chemical engineering, the modeling of packed-bed reactors, especially those with low-tube-to particle diameter ratio, which are used for highly exothermal reactions, has been studied extensively (see e.g., Nijemeisland and Dixon[5]). Another area of interest is the impregnation of fabrics during composites manufacturing,[6–10] in which the flow is often on several scales and different kinds of particles may be added to the fluid to add functionality to the molded composite. Manufacturing of new biocomposites and papermaking are other examples where dispersion matters.[11–14]

One way to numerically study the flow through fixed beds of spheres is to use traditional Computational Fluid Dynamics (CFD). The flow in fixed-bed reactors has, for example, been simulated with CFD with usage of finite volume discretization of the Navier–Stokes equations (see e.g., Refs. 5,15, and 16). Another approach for complex flow systems is the Lattice–Boltzman method,[17,18] that has been used to derive the detailed flow in porous media and in fixed-bed reactors (see e.g., Refs. 19 and 20) even for moderate Reynolds numbers. However, it may not be well suited for curved particle interfaces and sharp spacing between the spherical particles. As an alternative approach, accelerated Stokesian dynamics method[21] can be applied, but it requires inverting large matrixes for increased number of particles. Thus, although such methods can be successfully used to simulate the flow and study transport/transfer properties in packed beds of particles, it may be difficult to study large systems due to mesh refinement problems and the requirements of large computational resources. Hence, many of the early simulations were performed on unit cells with periodic boundary conditions.[22,23] Today, despite the advances of computational power, CFD simulation of a large number of particles often becomes very time consuming and expensive. In addition, there are certain difficulties related to the discretization of small distances near the particle-particle and particle-wall contact points. Therefore, the suitability of the mesh in general and particularly near these contact points should be analyzed carefully and methods should be developed that are stable regarding convergence, computational efficient and that has a geometrical configuration that can be altered in a simple way,[24,25] for example, due to deformations of porous media. Following these demands, a three-dimensional (3-D) porous-medium model is here built that consists of thousands of spherical particles that are divided into cells using Voronoi diagrams. The aim of building this model is to reproduce

Correspondence concerning this article should be addressed to T. S. Lundström at Staffan.Lundstrom@ltu.se.

mass transfer in a tracer column experiment and the resulting effluent curves. The dispersion is obtained by fitting the continuous model to either effluent curves or spatial distribution of the concentration front inside the column. It requires transient calculations that are less efficient than methods employing B-field[26] or other methods. However, with the approach it is possible to examine how the fitted dispersion develops as the concentration front moves inside the column. Of particular interest is the behavior at the inlet of the column where the discrete character of the particles can change the continuous interpretation of dispersion. On the other hand, it is still not clear whether the dispersion stabilizes if the column length increases depending on the condition at the side walls. Therefore, a study of a prolonged system is carried out.

The 3-D packed-bed model consists of thousands of randomly distributed spheres. Voronoi diagrams are applied to discretize the system into cells that each contains one sphere and Laurent series are applied to find the local flow fields inside the Delaunay tetrahedrons. The whole flow pattern is then obtained by minimization of the dissipation rate of energy[27,28] for the dual stream function.[29] The obtained stream function provides an excellent tool for flow visualization in porous media. As a result, a discretized 3-D packed-bed model is obtained that is employed to derive the longitudinal (D_L) and transverse (D_T) dispersion coefficients. The results are presented as D_L/D_m and D_T/D_m vs. $\mathrm{Pe_m}$ ($= ud/D_m$), and are further compared to experimental results from the literature. In these expressions, D_m is the molecular diffusion coefficient; d is the inert sphere diameter; and u is the average interstitial liquid velocity, defined as $u = U/\varepsilon$, where U is the superficial velocity and ε is the porosity. The flow rate in this study is limited to $\mathrm{Pe_m} < 10$ to analyze the dynamics in the tracer column experiment rather than to obtain the dispersion directly. At this range of velocities, the dispersion predominantly depends on the flow variation due to random packing of the porous media rather than variation of flow velocity between single solid particles, so called Taylor dispersion.[30,31] The Taylor dispersion is essential for higher velocities, that is, $\mathrm{Pe_m} > 10$. As only the low Reynolds number flows are considered, the boundary layer dispersion[30] is neglected. The boundary layer dispersion occurs at $\mathrm{Pe_m} \gg 1$ and results from tracers that come close to no-slip solid boundaries in the medium that could not escape the slow moving region near the boundary without the aid of molecular diffusion.[30]

This work is founded on an earlier published article[32] that used a 2-D packed-bed model to derive the dispersion coefficients. Moreover, similar to the previous 2-D packed-bed model,[32] the model derived herein is generic and can be applied to a number of areas of application such as investigations of the effects of particle-size distribution on the D_L,[33] drying of iron ore pellets,[34] filtration mechanisms during composites manufacturing,[35] and internal erosion processes.[36]

Numerical Setup

The type of packing in fixed beds affects the local fluid, heat, and mass transport,[37] and, thus, influences macroscopic variables such as dispersion coefficients and permeability. Therefore, the porous-medium model is used to derive the dispersion coefficients for a randomly packed bed, as well as for a bed with the same porosity and size distribution of spheres, but that is packed regularly (hexagonal close-packed). Most of the simulations that have been performed to study the flow and derive the dispersion coefficients in fixed beds of spheres use a fixed ε. However, the values of ε for a real packing of spheres are typically between 0.36–0.42[37] validating a study of the effects of ε in this range on the dispersion coefficients. The methodology used in this article to make a random packing of spheres, discretize the system of spheres, find the flow pattern in the packed-bed model and derive dispersion coefficients is robust and easy to implement.

Packing procedure

In general, the distribution of particles in natural systems has a random character. The porosity in such systems of equal-sized spherical particles varies typically from 36% to 42%. This is far from the minimum possible porosity of $1-\frac{\pi}{3\sqrt{2}} \approx 26\%$ for the densest periodic packing. Hence, there is a structural difference between these two packing, implying that the transfer from a periodic system to a random one is not straightforward.[38] One way to get a random close-packing structure is to generate a dilute nonoverlapping configuration. Then, an optimization procedure is launched, where the particles are subjected to a random motion and the overall distance between the particles is minimized.[39] Another way is to use a raining process, in which new particles are inserted from a random position at the top of a predefined volume and are subsequently allowed to fall into local minima.[20,40] This, however, does not give low enough porosities. A third alternative is to use the Jodrey–Tory algorithm that is based on "repulsion" of overlapping spheres with a gradual reduction of their radii.[41,42] A fourth route is the Lubachevsky–Stillinger algorithm, where molecular dynamics are used on nonoverlapping spheres, each having a radius that is allowed to gradually increase.[43] In the current case, the packing procedure should be able to handle fixed-sized systems with very low random porosities without any usage of non-natural forces. To meet these requirements, an initial random distribution of overlapping particles is generated. The quantity of particles corresponds to the intended porosity of nonoverlapping particles. Then, the system is virtually shaken until none of the particles overlap the others. The shaking of the system is made by a kind of Brownian motion, whereby particles can jump in a random direction at a random but small length in each step.[44] However, the jumps that increase overlapping of the particles are set to be less frequent, W_+, compared to jumps that decrease or do not change overlapping, W_{0-}, according to a piecewise simulated annealing technique: $W_+/W_{0-} = (1-\mathrm{frac}\left[(i/i_0)^2\right])\exp\left[-i/i_1\right]$, where i is index of iteration, frac denotes fractional part, i_0 and i_1 are parameters that are chosen to be around 10^4. It is clear that the shaking time increases as a function of final particle fraction of the system. The shaking is stopped as soon as a nonoverlapping configuration of particles is reached resulting in a practically consolidated porous media. The default porosity in the current study is 40%, which requires typically less than 10^4 jumps for each particle. However, as the porosity decreases the required number of jumps increases considerably. The minimum bulk porosity is, as previously stated, 36% for uniform-sized spheres.[37] In this article, the lowest porosity studied for equal-sized particles is 36.5%. It is possible to obtain lower porosities for random systems for

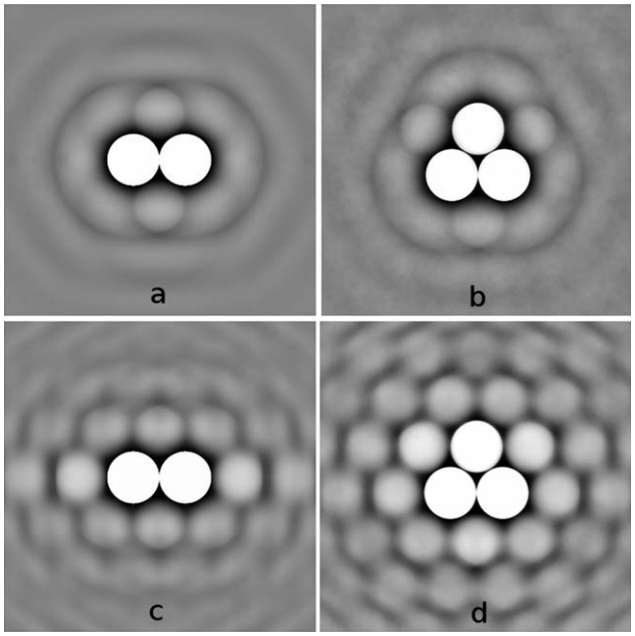

Figure 1. Correlation functions for large random (a and b) and perturbed regular hexagonal close-packed (c and d) systems with equal-sized particles and porosity of 0.4: (a and c) around 2 close-spaced particles in axial cross section, and (b and d) around 3 close-spaced particles in the plane of particles.

White represents zero porosity, black—porosity equal to one, that is, particles are absent at that location. Grey is porosity between these values.

different-sized particles, as the smaller particles can partially fill the spaces between larger particles.

As previously mentioned two types of packing were used in this study; random and perturbed regular hexagonal close packing (hcp). Note that the perturbations to regular packing are introduced because otherwise the Delaunay tessellation described in the next section would degenerate, that is, there are several ways to construct the Delaunay tessellation upon the same Delaunay criterion. Moreover, the current method is not well suited for completely regular packing as higher flow rate effects can be important already at smaller Pe_m. To exemplify the difference between the two packing, the correlation functions around two and three close-spaced particles for these systems are plotted in Figure 1, that is, porosity as function from the distance from the selected particles. White represents zero porosity, that is, there is certainly a particle at this relative position, whereas black represents relative position where no particle is present. For the random system, the oscillations of average statistical porosity at a given distance from the reference particles quickly cease and become the average porosity of the system; see Figures 1a, b. Nevertheless, there are positions close to the reference particles where there is a high probability of having a particle. In the case of perturbed regular packed system, however, the oscillations of average statistical porosity are substantial even at a rather large distance from the reference particles, as clearly seen in Figures 1c, d.

Voronoi discretization of the random system

The complete system has to be divided into smaller parts to build a discrete numerical scheme. Using Voronoi diagrams, the system of particles is divided into cells that each contain one particle; see Figure 2. The general methodology is based on the fast Bowyer-Watson algorithm as in Thompson[45] but with another initial tessellation. Voronoi diagrams are mutually related to Delaunay tessellation. Following Thompson,[45] the primary system is surrounded by 26 equal systems or domains to deal with the periodic boundary conditions for the Delaunay tessellation. A tetrahedron that connects the four closest particles can be such that the particles belong to different domains at the boundary of the system. Therefore, the particles in the tetrahedron have a position in the primary system as well as in the domain that they belong to. As the tetrahedrons are the same in each domain, only tetrahedrons with the lowest index particle in the primary system need to be considered. Tessellation in this study starts from just one particle in the primary domain with six tetrahedrons, whereas Thompson[45] used eight initial particles in the primary domain near the eight corners of the system to get an initial tessellation with 40 tetrahedrons. A parallelepiped may also be divided into five tetrahedrons, but this would destroy the periodicity, as each face of the tetrahedron should contact the same face of another tetrahedron either from the primary domain or neighboring domain. As the system in this study can have very different dimensions in different directions, tetrahedrons at the initial stage of the algorithm are nearly degenerated and may introduce numerical instabilities. If particles that are well inside an existing base tetrahedron are accounted for, then even more degenerate tetrahedrons could be created. It is therefore better to first select the particles that cross or are very close to the existing long faces of Delaunay tetrahedrons. Then, both facing tetrahedrons will definitely be included in the core according to the Delaunay criterion and the new tetrahedrons will be less

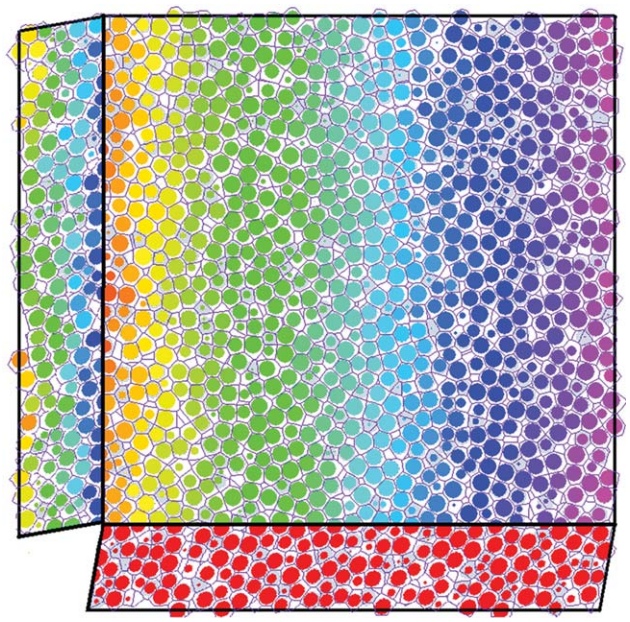

Figure 2. Example of a Voronoi mesh of a 3-D system with dimensions 0.36 × 0.06 × 0.36 m^3 and with 5157 particles.

Cross sections in the *x-z* plane (main part), *y-z* plane (left), and *x-y* plane (bottom) are shown. Shaded particles have the center behind the cross section, the others in front of it. The color represents component of the stream function for each particle perpendicular to the corresponding cross section.

degenerate. Unlike Thompson,[45] the visibility test and lost vertex-test of the core is performed at each insertion of the new tetrahedron,[46] as opposed to afterward. Notice that the discretization of Voronoi cells is strictly defined by the mutual Delaunay tessellation and no grid refinement study can be performed at this stage.

Derivation of dual stream function

To simulate a tracer column experiment, to obtain the resulting effluent curves and dispersion coefficients, the flow field must be known for the complete system, for a certain configuration of particles. As the liquid is considered to be incompressible, the stream function and vorticity approach has certain benefits, such as automatic conservation of the continuity equation. The stream function, $\boldsymbol{\psi}$, and the vorticity, $\boldsymbol{\omega}$, are vectors with three components, making the derivation of the flow field rather difficult but still possible to carry out. The stream function $\boldsymbol{\psi}$ is not strictly defined, as there are a number of possibilities to obtain the same velocity distribution

$$\mathbf{u}=\nabla\times\boldsymbol{\psi} \tag{1}$$

In analogy with the magnetic vector potential, the following assumption is hypothetically useful

$$\nabla\boldsymbol{\psi}=0 \tag{2}$$

as it makes it possible to express $\boldsymbol{\omega}$ as

$$\boldsymbol{\omega}=\nabla\times\mathbf{u}=\nabla\times(\nabla\times\boldsymbol{\psi})=-\nabla^2\boldsymbol{\psi} \tag{3}$$

where a vector component of $\boldsymbol{\omega}$ is related only to the same vector component of $\boldsymbol{\psi}$ in Cartesian coordinates. The coupling of the vector components is then realized through the constraint (2). For low Reynolds numbers (Re), the energy dissipation rate tends to decrease to a minimum[27,28] (see Appendix A). This can be expressed in the following manner

$$\int \mu\boldsymbol{\omega}^2 dV=\min \tag{4}$$

where μ is the fluid dynamic viscosity and the integral is taken over the total volume of the system. Assume a large porous system in the form of a rectangular parallelepiped according to

$$\begin{cases} 0\le x\le a_x \\ 0\le y\le a_y \\ 0\le z\le a_z \end{cases} \tag{5}$$

with a superficial velocity U directed along the z axis. Proper boundary conditions should be specified for $\boldsymbol{\psi}$ that yield the superficial velocity U, agreeing with the periodic boundary conditions for velocity, and fulfill constraint (2). One possibility is to set the following conditions

$$\begin{cases} \psi_x(0,y,z)=\psi_x(a_x,y,z), \quad \psi_y(0,y,z)=\psi_y(a_x,y,z)-\dfrac{a_xU}{2}, \quad \psi_z(0,y,z)=\psi_z(a_x,y,z) \\ \psi_x(x,0,z)=\psi_x(x,a_y,z)+\dfrac{a_yU}{2}, \quad \psi_y(x,0,z)=\psi_y(x,a_y,z), \quad \psi_z(x,0,z)=\psi_z(x,a_y,z) \\ \psi_x(x,y,0)=\psi_x(x,y,a_z), \quad \psi_y(x,y,0)=\psi_y(x,y,a_z), \quad \psi_z(x,y,0)=\psi_z(x,y,a_z) \end{cases} \tag{6}$$

Then, the linear system of equations with respect to $\boldsymbol{\psi}$ can be solved independently as previously done in the 2-D case.[32] Evaluating the z-component of $\boldsymbol{\psi}$, it is clear that the trivial solution $\psi_z=0$ both satisfies the boundary conditions (6) and minimizes (4), which is another possible constraint for $\boldsymbol{\psi}$ instead of Eq. 2. Following this finding, the 3-D flow field can be described by just two components of $\boldsymbol{\psi}$, namely x and y. This is often called the dual stream function approach, which can in principle represent any 3-D Stokesian flow in a porous media.[29] This methodology is used in this article and the example of a dual stream function is illustrated in Figure 2.

Local flow around particles

The spherical particles are assumed to be impermeable; therefore, $\boldsymbol{\psi}$ can be assumed constant inside the particles. Moreover, the boundaries of the solid particles have nonslip boundary conditions. Therefore, the change of $\boldsymbol{\psi}$ is infinitesimal at the surface of each particle and the local $\boldsymbol{\psi}$ varies only in the space between particles.

Consider a Delaunay tetrahedron that has four faces with each face consisting of three spherical particles. If the tetrahedron has a dense packing, then there are channel-like openings through each one of the faces. The flow distribution in it can be derived as in a channel with a slowly varying shape along its length. The assumption is valid also if the particles are not completely compact, which results in a shape of the cross-section channel as in Figure 3. The cross section can be further separated into six sections (see Figure 3), that is, two sections per particle. If the cross section forms a regular triangle, then the flow pattern for a velocity component normal to the cross section can be obtained by a Laurent series according to

$$\mathrm{u}=\mathrm{A}\left(\frac{R^2-r^2}{4}+B_0\,ln\frac{r}{R_0}+\sum_{n=1}^{\infty}B_n\left[\left(\frac{R_0}{r}\right)^{\mathrm{kn}}-\left(\frac{r}{R_0}\right)^{\mathrm{kn}}\right]\cos\left[\mathrm{kn}\phi\right]\right) \tag{7}$$

In this equation, R is the polar radius of the particle as viewed in the given cross section; r and ϕ are polar coordinates with respect to the reference point in the center of the particle; A, B_0, and B_n are constants; and k is the order of rotational symmetry, which for a regular triangle is 6, that is, six regular triangles fit around one particle in the given plane. The Laurent series automatically satisfies the viscous-flow equation for the velocity component u normal to the cross section according to

$$\Delta u=-A \tag{8}$$

This relationship is true for any constants B_0 and B_n.[47] Moreover, the nonslip boundary condition and $\varphi=const$ at the surface of the spheres are automatically satisfied. The constants B_0 and B_n should be chosen to fit the boundary condition at $r\cos\varphi=x_0$, where x_0 is the position of the Voronoi surface as viewed from the particle. The summation

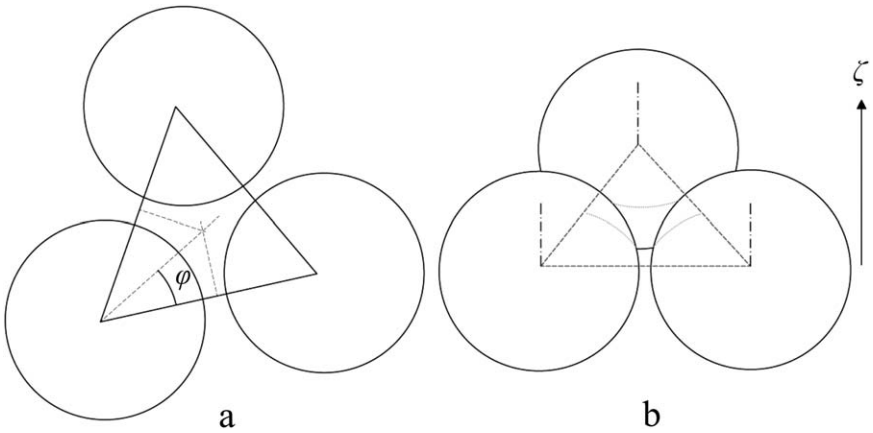

Figure 3. (a) Division of the cross section between three particles in triangles, and (b) cross section of the space between three spheres.

over n in the Laurent series, Eq. 7, convergences very quickly, especially with less dense packing.[40] Therefore, it is adequate to take into account only the first few terms ($n = 1$, 2, 3) in the summation. Equation 7 is extended to a general case of a nonregular triangle, where the circumcenter of the triangle takes the role of the center point. The order of rotational symmetry, k, is not an integer for the irregular case, but is a reciprocal of the angle of the triangle: $k = \frac{\pi}{\Delta\varphi}$.

The total flow through the face of the triangle can be expressed by a contour integral of ψ over the perimeter of the cross section in the following manner

$$\int \mathbf{u} d\mathbf{S} = \oint \psi d\mathbf{l} \tag{9}$$

This makes it possible to determine the proportionality constant A. The vorticity can be readily calculated from Eq. 7 by differentiation. Thus, the integral of the dissipation rate of energy, Eq. 4, in a tetrahedron can be expressed in a quadratic form

$$\int_{\text{tetrahedron}} \boldsymbol{\omega}^2 dV = \sum_{i=1}^{4}\sum_{j=1}^{4} C_{ij}\left(\oint \psi d\mathbf{l}\right)_i \left(\oint \psi d\mathbf{l}\right)_j \tag{10}$$

where $\left(\oint \psi d\mathbf{l}\right)_i$ is the total flow through the i-face of the tetrahedron, and $C_{ij} = C_{ji}$ are coefficients for the particular shape of the tetrahedron. The diagonal terms C_{ii} dominate for compact packing. The volume integral of ψ derived from Laurent series (Eq. 7) enables the derivation of these coefficients. The other option would be to use CFD to obtain the coefficients C_{ij}. This will be accomplished in later studies enabling an estimation of the accuracy of the present approach. The distribution of ψ follows from the minimization of the total dissipation rate of energy, which creates a system of linear equations. The stream function methodology makes it possible to include the convection directly by usage of the integral of ψ over the perimeter of each Delaunay face. This gives the total mass flow through the Delaunay tetrahedron according to Eq. 9. The total convection pattern is obtained by combining all tetrahedrons.

To test the flow solution as well as the packing generation method, the relationship between permeability and porosity in the present packed-bed model is compared to the Rump and Gupte's formula for packed beds of spheres, see Appendix B. As can be seen in Appendix B, the obtained permeability data fits well with Rumpf and Gupte's formula.

Molecular diffusion

The molecular diffusion needs to be included in the model as well. As the considered flow rate is low, $\mathrm{Pe_m} < 10$, then a simplified version of the diffusion can be applied as the effects of Taylor and boundary layer dispersion[30,31] starts to appear at higher flow rates. Molecular diffusion occurs primarily along the Voronoi faces. The vertex of each Voronoi face is the circumcenter of the corresponding Delaunay tetrahedron. Thus, the flow between two neighboring vertices goes through the face of three spheres of the corresponding tetrahedrons; see Figure 3b. The narrow gap between three spheres has a channel-like form with varying area of the cross section, $S(\xi)$, with the smallest area at $\xi = 0$ when $S(\xi) = S_0$. If the absolute value of ξ is equal to the radius of the spheres, then the spheres do not reduce the area S and the maximum area, $S_{\max}$, is obtained. In other cases, the area $S(\xi)$ is

$$S(\xi) = S_{\max} - \frac{1}{2}\sum_{k=1}^{3}\alpha_k(R^2 - \xi^2) = S_0 + \frac{1}{2}\sum_{k=1}^{3}\alpha_k\xi^2 \equiv S_0 + \Lambda\xi^2 \tag{11}$$

where α_k is angle of the triangle at corresponding sphere, $S_0 = S_{\max} - \frac{1}{2}\sum_{k=1}^{3}\alpha_k R^2$, and $\Lambda = \frac{1}{2}\sum_{k=1}^{3}\alpha_k = \frac{\pi}{2}$. The total mass-transfer resistance to molecular diffusion between vertices with coordinates ξ_1 and ξ_2, through these three spheres in such a 1-D channel approach is

$$\frac{1}{D}\int_{\xi_1}^{\xi_2}\frac{1}{S(\xi)}d\xi = \frac{1}{D}\frac{1}{\sqrt{S_0\Lambda}}\arctan\left[\sqrt{\frac{\Lambda}{S_0}}\xi\right]\Bigg|_{\xi_1}^{\xi_2} \tag{12}$$

The flow rate through the same face of three triangles is given by an integral (9) where the integration is taken along the perimeter of the triangle. Thus, the mass transport between two adjacent vertices can be calculated. Then, by collecting all of the adjacent pairs of vertices, the global mass transport is obtained.

Longitudinal dispersion

To compute D_L, a breakthrough experiment is simulated in a rectangular parallelepiped consisting of discrete randomly packed spherical particles, in which the main flow is directed upward. The 1-D problem for a system with a constant D_L, fixed concentration, c_0, at the inlet, and flux free concentration at the outlet is

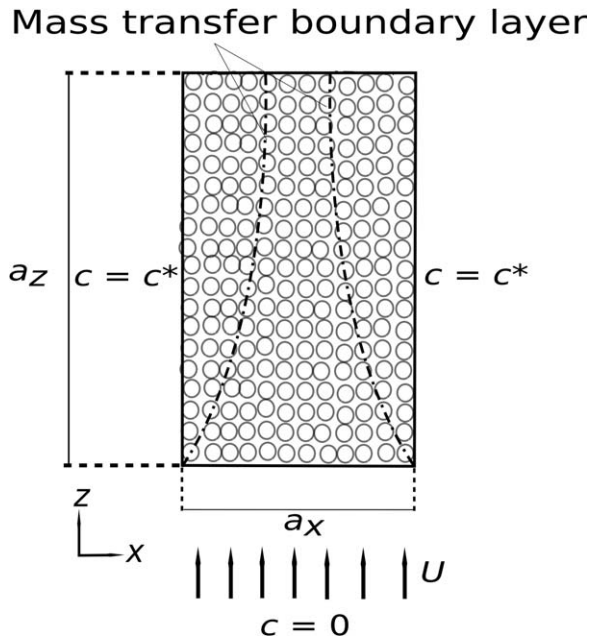

Figure 4. Schematic representation of the transverse dispersion simulation setup, cross section in the *x-z* plane.

$$\frac{\partial c}{\partial t}+u\frac{\partial c}{\partial z}=D_L\frac{\partial^2 c}{\partial z^2}, \tag{13}$$

$$\begin{aligned} &c=0, \quad 0<z\le L, \quad t=0\\ &c=c_0, \quad z=0, \quad t\ge 0,\\ &\frac{\partial c}{\partial z}=0 \quad z=L, \quad t\ge 0 \end{aligned} \tag{14}$$

where c is the mean solute concentration, t is time, z is the distance in the main flow direction, and L is the length of the packed bed. Equation 13 with boundary conditions (14) has the following approximate analytical solution[48]

$$\begin{aligned} \frac{c}{c_0}&=\frac{1}{2}\mathrm{erfc}\left(\frac{z-ut}{2\sqrt{D_L t}}\right)+\frac{1}{2}\exp\left(\frac{uz}{D_L}\right)\mathrm{erfc}\left(\frac{z+ut}{2\sqrt{D_L t}}\right)\\ &+\frac{1}{2}\left[2+\frac{u(2L-z)}{D_L}+\frac{u^2 t}{D_L}\right]\exp\left(\frac{uL}{D_L}\right)\mathrm{erfc}\left(\frac{2L-z+ut}{2\sqrt{D_L t}}\right)\\ &-\sqrt{\frac{u^2 t}{\pi D_L}}\exp\left[\frac{uL}{D_L}-\frac{(2L-z+ut)^2}{4D_L t}\right] \end{aligned} \tag{15}$$

The 1-D profile of the concentration front is calculated as volume-averaged $\langle c\rangle_{\mathrm{vol}}(z,t)=\frac{1}{S\Delta z}\int_{z-\Delta z/2}^{z+\Delta z/2}\left(\iint_S c(x,y,z,t)dxdy\right)dz$, and flow-averaged, $\langle c\rangle_{fl}(z,t)=\iint_S c(x,y,z,t)u_z(x,y,z,t)dxdy/\iint_S u_z(x,y,z,t)dxdy$, where Δz is a small interval in the main flow direction used for the volume averaging, and S represents the area of the cross section of the system perpendicular to the flow direction. D_L is then obtained by fitting (15) to this 1-D concentration profile for fixed u. The choice of using the fixed u and the method used to fit (15) to the concentration profile is discussed in Jourak et al.[32] The side walls of the 3-D packed-bed model have periodic boundary conditions; therefore, the D_L that is obtained in this study corresponds to the bulk dispersion without influence from the walls.

Transverse dispersion

Focus here is set on a 3-D rectangular parallelepiped with a fixed concentration of a substance on the walls parallel to the main flow field. The D_T is then derived by computing the extension of the concentration from the walls. Figure 4 depicts a schematic representation of the transverse dispersion simulation setup in the x-z cross section. This method is similar to that developed by Coelho and Guedes de Carvalho,[49] and is explained, in detail, in a previously published 2-D study.[32]

System setup

The parameters of the setups that were used for the simulations are shown in Tables 1 and 2. The flow was Stokesian for all the setups. The standard porosity of the system was 0.40. However, to study the effects of porosity on the dispersion coefficients, porosities in the range of 0.365–0.45 were also used. This is the range of ε typically observed in real beds of spheres.[37] Moreover, the effects of packing structure on the dispersion coefficients were studied by comparing the randomly packed systems to their counterparts that had been packed regularly (hexagonal close packed). The diameter of the uniform-sized spheres that were used in the present study was 12 mm. The numerical transient solution takes less than 1 day on a single core standard computer. Instead, most of the computing time is spent on the packing procedure especially for the denser packing.

Results and Discussion

For $\mathrm{Pe_m}<0.4$, molecular diffusion dominates and $D_L<D_m$, due to the tortuosity of the porous medium.[50]

Table 1. Longitudinal Dispersion Simulations

Case	System Size Width × Depth × Length (m^3)	ε	τ	D_L/D_m at $\mathrm{Pe_m}=0.01$	D_L/D_m at $\mathrm{Pe_m}=0.1$	D_L/D_m at $\mathrm{Pe_m}=1$	D_L/D_m at $\mathrm{Pe_m}=10$
A1–5	0.12 × 0.12 × 0.50	0.40	1.45	0.688 ± 0.003	0.697 ± 0.006	0.802 ± 0.006	2.76 ± 0.03
B	0.12 × 0.12 × 1.0	0.40	1.45	0.688	0.695	0.800	2.77
C1–5	0.10 × 0.10 × 1.0	0.40	1.45	0.690 ± 0.003	0.697 ± 0.004	0.804 ± 0.005	2.76 ± 0.03
D1–6	0.07 × 0.07 × 1.0	0.40	1.45	0.687 ± 0.004	0.696 ± 0.006	0.802 ± 0.005	2.82 ± 0.08
E	0.07 × 0.07 × 1.5	0.40	1.45	0.690	0.701	0.810	2.80
F1–6	0.07 × 0.07 × 2.0	0.40	1.45	0.689 ± 0.004	0.703 ± 0.007	0.814 ± 0.007	2.83 ± 0.03
G	0.10 × 0.10 × 1.0	0.45	1.41	0.707	0.713	0.829	2.90
H	0.10 × 0.10 × 1.0	0.39	1.46	0.685	0.689	0.794	2.78
I	0.10 × 0.10 × 1.0	0.37	1.48	0.674	0.680	0.782	2.72
J	0.10 × 0.10 × 1.0	0.365	1.49	0.669	0.677	0.779	2.72
*K	0.10 × 0.10 × 1.0	0.40	1.29	0.773	0.782	0.852	2.27

*Packing structure is perturbed regular hexagonal close-packed (hcp). The D_T/D_m values are nondimensional transverse dispersion coefficients obtained from the effluent curves. The values behind "±" are standard deviations for the given number of simulations. ε is the porosity and τ is the tortuosity factor.

Table 2. Transverse Dispersion Simulations

Case	System Size Width × Depth × Length [m^3]	ε	τ	D_T/D_m at $Pe_m=1$	D_T/D_m at $Pe_m=10$	D_T/D_m at $Pe_m=100$
L1–6	0.18 × 0.18 × 0.18	0.40	1.49	0.87 ± 0.01	2.7 ± 0.1	21 ± 1
M1–6	0.36 × 0.06 × 0.36	0.40	1.41	0.85 ± 0.02	2.3 ± 0.1	18 ± 1
N	0.50 × 0.04 × 0.50	0.40	1.40	0.84	2.3	17
O	0.50 × 0.04 × 0.50	0.45	1.38	0.89	2.5	19
*P	0.40 × 0.07 × 0.40	0.40	1.36	0.91	1.8	9.50

*Packing structure is perturbed regular hexagonal close-packed (hcp). The D_T/D_m values are nondimensional transverse dispersion coefficients. The values behind "±" are standard deviations for the given number of simulations. ε is the porosity and τ is the tortuosity factor.

Figure 5a exemplifies this condition at $Pe_m = 0.1$ for a simulation of longitudinal dispersion. Increasing Pe_m to 10, which implies an increase in the velocity, makes the concentration gradient much steeper; compare Figures 5a, b. For transverse dispersion, an increase in Pe_m from 1 to 10 results in a steeper concentration gradient at the wall; compare Figures 5c, d. Hence, the concentration gradients are highly dependent on the velocity of the fluid in the range studied.

Estimation of D_L

The estimation of D_L is rather straight forward as described in the previous section and in Jourak et al.[32] Transient longitudinal dispersion simulations of the breakthrough column experiments were performed in the 3-D packed-bed model. From these simulations, the 1-D concentration profiles can be derived, as described earlier. Figure 6 provides an example of the concentration profiles within a porous medium for setup C, in which the values of D_L/D_m are shown beside each respective curve. These values of D_L/D_m were estimated by fitting Eq. 15 to the concentration distributions (solid lines). Due to the unevenness of the flow front, the concentration may vary at any cross section perpendicular to the main flow direction (z axis), at a given time. This variation of concentration is indicated as error bars in Figure 6. A larger unevenness is characterized with longer error bars. Note that for the previous 2-D packed-bed

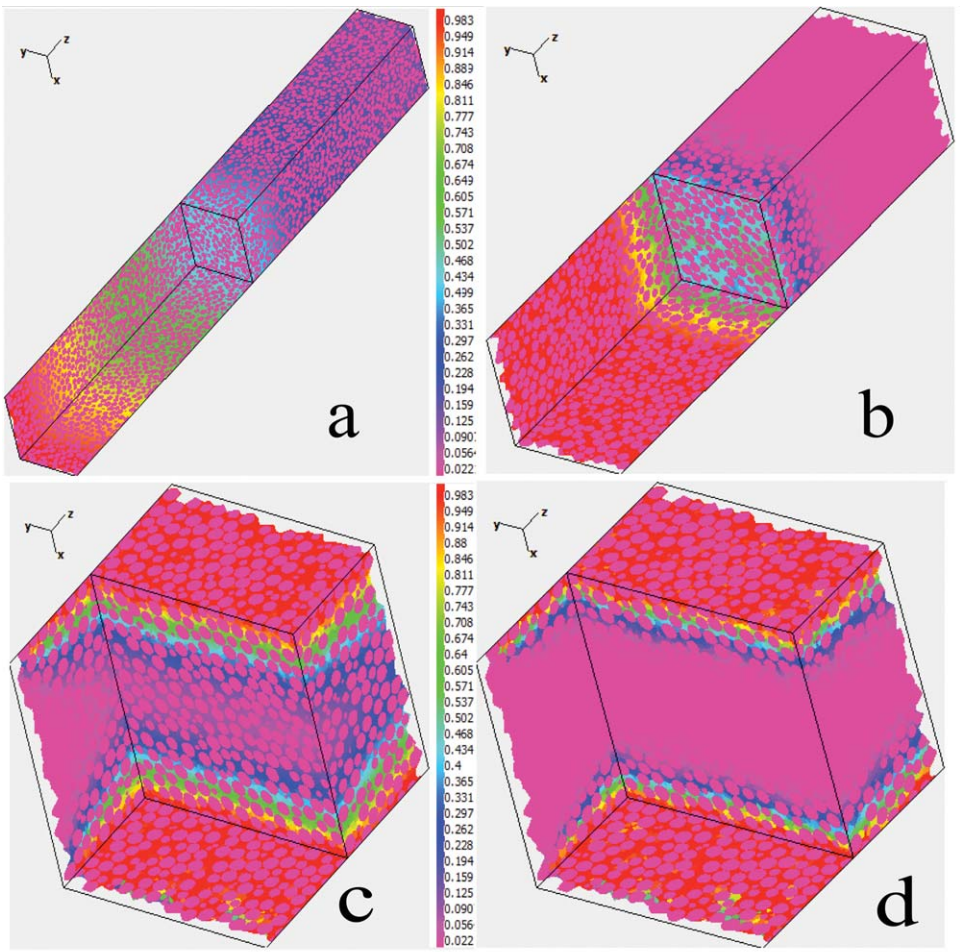

Figure 5. Concentration distributions for the derivation of D_L (snapshots): (a) $Pe_m = 0.1$, Case B, (b) $Pe_m = 10$, Case A.

Final concentration distributions for case L for the calculation of D_T : (c) $Pe_m = 1$, (d) $Pe_m = 10$. The color represents the magnitude of nondimensional concentration (i.e., c/c_0) as it can be seen from the legend. Violet circles are cross sections of spheres at the given planes.

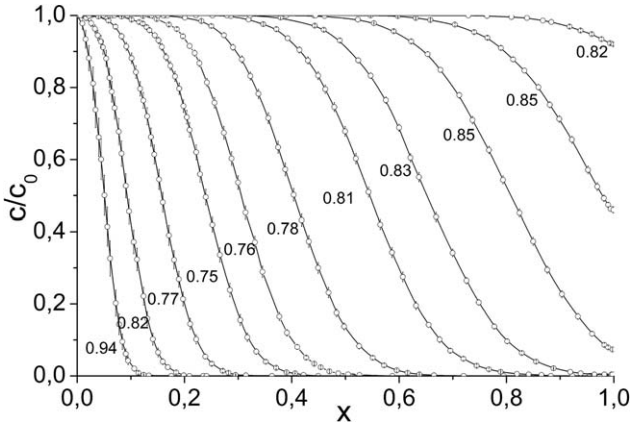

Figure 6. Flow-averaged (o) concentration profiles at various times vs. distance in the packed bed for simulation C at Pe_m = 1.

The error bars represent statistical variation of the concentration at a given cross section perpendicular to the z axis. The solid lines represent an approximation via the analytic formula (16). The values of the estimated D_L/D_m are shown beside their respective curves.

model (see Figure 4 in Jourak et al.[32]) the error bars were typically longer than the present case. This result is predicted and is related to the extradimension that the flow can use in 3-D as compared to 2-D, resulting in a smoother flow front. The irregularity of the concentration gradient can also be examined by plotting the variation of the maximal standard deviation of the relative concentration in one cross section vs. time; see Figure 7 for case C and K. This value is in the range of 0–0.5, where the latter corresponds to the theoretical situation when half of the cross section has concentration 0 and the other half c_0. For a consistent result, the maximal standard deviation should with time go toward a lowest possible value at one pore volume (= tu/L). The reason for this is that the extent of the concentration gradient increases in

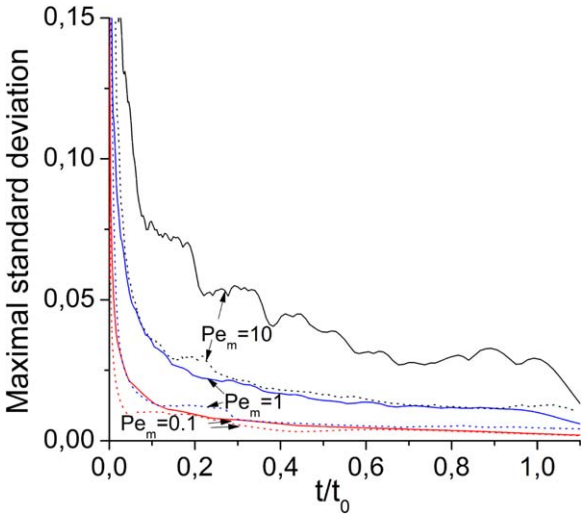

Figure 7. Variation of the maximal standard deviation in one cross section normal to the z axis vs. nondimensional time for case C (solid line) and for case K, hexagonal close-packed packing (dotted) at different Pe_m values; $t_0 = L/u$.

[Color figure can be viewed in the online issue, which is available at wileyonlinelibrary.com.]

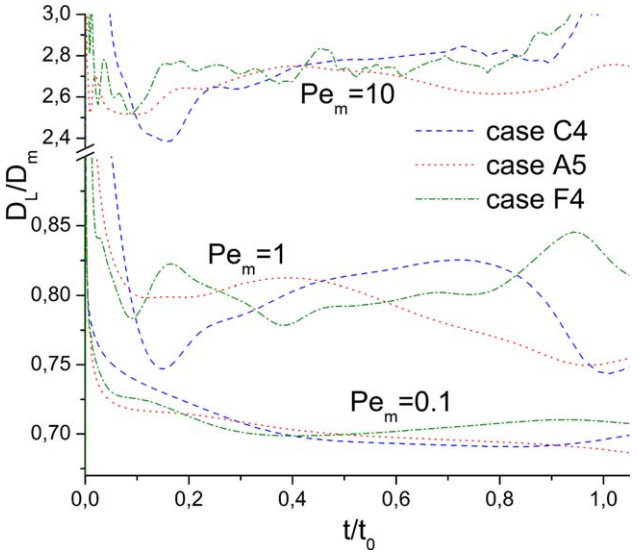

Figure 8. The development of the nondimensional longitudinal dispersion coefficients (obtained from flow-averaged concentration profiles) at different Pe_m vs. nondimensional time; $t_0 = L/u$.

[Color figure can be viewed in the online issue, which is available at wileyonlinelibrary.com.]

the longitudinal direction within the packed bed as the flow evolves and moves toward the end of the bed. This results in less variation of concentration in the perpendicular direction. As can be seen from Figure 7, the perturbed regular packing, case K, has a more even concentration gradient compared to the full random packing, case C. It is clear that the increase of velocity amplifies the unevenness of the flow front; see Figure 7.

Figure 8 shows the development of D_L/D_m as a function of nondimensional time obtained by fitting Eq. A1 to the concentration distributions during transient simulations. The simulations are performed for different sizes of the system, where case A is the shortest and thickest system and case F is the longest and thinnest one. For a randomly packed (uniform-size packing) homogenous packed bed, without structural variety as for all cases in this article, D_L should stabilize within the porous medium, as long as the system is sufficiently long.[51] As can be seen from Figure 8, the length of the systems should be as long as possible to reduce natural fluctuations of D_L far from the inlet and outlet. However, the fluctuations of D_L increase when the Pe_m increases (see Figure 8). Therefore, for a monosized particle packed bed, the higher Pe_m the longer the required system to achieve a constant longitudinal dispersivity.[51] Note that the reasons for the initial peaks as well as the sudden increase of fluctuations of D_L/D_m toward the end of the packed bed in Figure 8 are explained in an earlier study.[32] The fluctuations continuous also at $t > t_0$ as the diffusion free boundary condition is specified at the outlet. The natural fluctuations due to the random configuration of particles can be reduced by studying huge systems of particles.

The estimated values of D_L were derived by fitting Eq. 15 to the obtained effluent curves from the packed-bed model, as it represents the average value that pertains to the whole length of the packed bed (see Figure 9). The effluent curves are obtained by plotting the averaged concentration at the outlet as function of time. The fitting to Eq. 15 is made by a least-square fitting procedure. For that reason, the discrete solution is discretized with 20 points along the ordinate axis

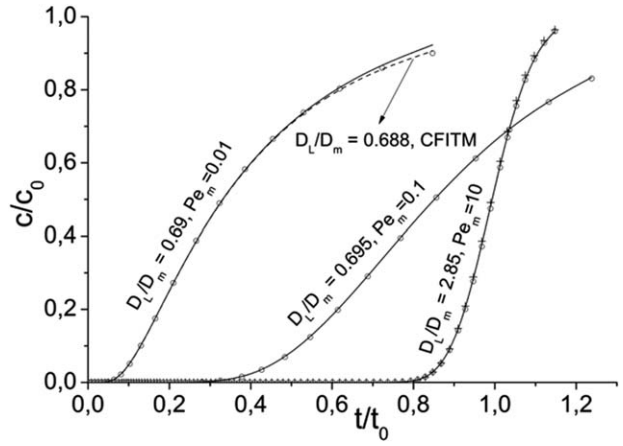

Figure 9. Flow-averaged (o) concentration effluent curves for simulation C vs. nondimensional time at $Pe_m = 0.01$, $Pe_m = 0.1$, and $Pe_m = 10$.

The solid lines represent approximations via the analytical formula (16). The volume-averaged concentration effluent curve (+) is shown as an example for $Pe_m = 10$. The dashed curve shows the fitted effluent curve via the CFITM code for $Pe_m = 0.01$; $t_0 = L/u$.

to find the best fit to the analytical solution. As can be seen from Figure 9, the flow-averaged and volume-averaged effluent curves nearly coincide. When either of the conditions, $uL/D_L > 100$ or $uL/D_L > 5 + 40\ ut/L$, are satisfied, Eq. 15 is a sufficient accurate approximation to Eq. 13 with boundary conditions from Eq. 14. For instance, as can be seen in Figure 9, Eq. 15 provides an excellent fit to all the effluent curves (solid lines) except at $Pe_m = 0.01$, where there is a minor deviation at larger times. To obtain an accurate value of D_L at this range, the CFITM code[52] within the STANDMODE software,[53] which includes the exact solution of Eq. 13 was applied (see dashed curve in Figure 9 for $Pe_m = 0.01$).

Parameter study

Results of the simulations are presented in Tables 1 and 2 and the estimated values of dispersion coefficients are presented as D_L/D_m and D_T/D_m vs. Pe_m in Figures 10 and 11, respectively. The effects of packing structure, porosity, and system size on dispersion coefficients are here examined.

Parameter study

Similar to the previous 2-D study,[32] variation of packing structure from random to regular packing changes the obtained dispersion coefficients noticeably. When the system was packed regularly, the tortuosity of the porous medium deceased and thus D_L and D_T increased at very low Pe_m (see differences at $Pe_m < 2$ between simulations C and K in Table 1 as well as F and K in Figure 10, and those between N and P in Table 2 and Figure 11). In the case of regular packing, the flow path is less tortuous, which in turn decreases the tortuosity of the porous medium.

At $Pe_m > 2$, however, the values of D_L and D_T are much lower for the regular systems compared to their counterparts for randomly packed systems; see the results for $Pe_m > 2$ between simulations F and K in Figure 10, and those between N and P in Figure 11. This is related to the lower dispersion associated with a less irregular flow front in the ordered structure system as in case K, which is clearly visible by the lower maximal standard deviation compared to the randomly packed system C in Figure 7 described earlier. For the regular case, there is an apparent anisotropy of the system related to orientation of the main flow direction with respect to the crystal orientation. The direction of the hcp crystal denoted by Miller index as [001] is oriented along the main stream direction (z axis) for longitudinal simulations and along x axis for transverse dispersion simulations. A large irregular packing, however, is almost isotropic and orientation could be arbitrary.

Parameter study

As the system becomes more densely packed, that is, the porosity of the medium decreases, the sinuosity of the flow path increases. Therefore, decreasing the porosity of the packed bed results in an increase of the tortuosity,[54] which in turn reduces the magnitudes of D_L and D_T in the molecular diffusion regime. Tables 1 and 2 provide comparison of the

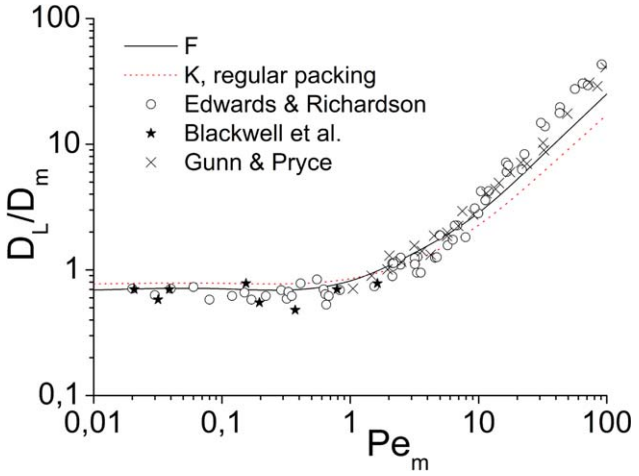

Figure 10. Computed D_L/D_m in a packed-bed model for simulations F and K in comparison to 3-D experimental data from Edwards and Richardson,[57] Blackwell et al.,[58] and Gunn and Pryce.[59]

[Color figure can be viewed in the online issue, which is available at wileyonlinelibrary.com.]

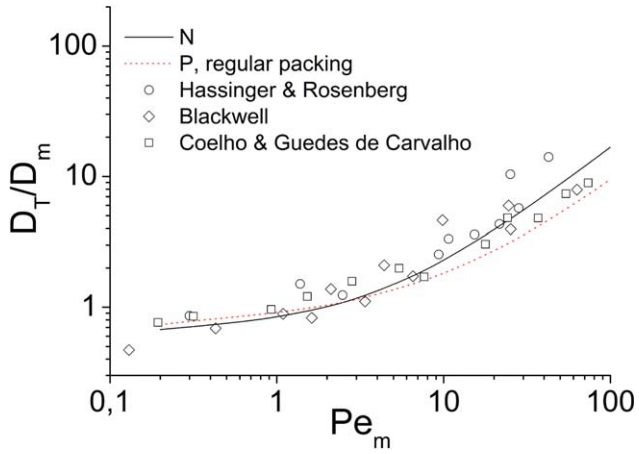

Figure 11. Computed D_T/D_m in a packed-bed model for simulations N and P in comparison to 3-D experimental data from Hassinger and Rosenberg,[55] Blackwell,[56] and Coelho and Guedes de Carvalho.[49]

[Color figure can be viewed in the online issue, which is available at wileyonlinelibrary.com.]

values of τ from longitudinal simulations of G to C; C to H; H to I, and I to J; and from transverse simulations of O to N. Nevertheless, at $Pe_m > 1$, the effect of porosity on dispersion coefficients is marginal, confirming results in the 2-D study.[32]

Parameter study

For the longitudinal dispersion simulations, increasing the cross section area of the system marginally decreases the statistical variations. See Table 1 for comparison of standard deviations between simulations C and D. As previously mentioned, for the D_L to stabilize within the packed-bed model, the system should be sufficiently long. Therefore, within the computational limit for a given number of spheres, to obtain a stabilized D_L, the system can be kept relatively narrow with periodic boundary conditions on the side walls to avoid wall effects, whereas the length of it should be as long as possible. The size of the packed bed and the number of spheres therein can be increased keeping in mind that simulation of a very large number of spheres is computationally expensive. In this study, at $Pe_m \leq 100$, however, for the given number of spheres, for example, around 7000 with the diameter of 12 mm, the length of 1 m is nearly sufficient, as the fluctuations of D_L within the packed bed far from the inlet and outlet are marginal (see Figure 8).

For the transversal dispersion simulations, the width (x-dimension) and length (z-dimension) of the system is more important than its depth (y-dimension). The reason is as the flow moves upward in the z-direction the solute is transversally dispersed mainly in the x-direction, due to the fixed concentration boundary condition at the side walls. Moreover, the D_T is derived from an approximate solution, which works best for large systems.[32] Therefore, the length and width of it should be as large as possible, whereas its depth can be kept relatively low. In this study, as the length and width of the system increase, the resulting D_T value decreases (see Table 2 for comparison between simulations L, M and N). As the derived D_T from simulation N is in good agreement with 3-D experimental data in the laminar flow regime,[49,55,56] it is believed that the size of system N is sufficient (see Figure 11).

Comparisons of derived D_L, D_T, and τ, to experimental data

The derived D_L and D_T are here validated with previously derived 3-D experimental data[49,55–59] from the literature in the laminar flow regime, that is, low Pe_m; see Figures 10 and 11. The present simulations are in good agreement with the 3-D experimental data. This suggests that the present approach to study flow and dispersion in 3-D packed beds of spheres in the laminar flow regime is acceptable. As a consequence of the random nature of the packing, and, thus, the uneven distribution of the flow, the mechanisms that cause dispersion in randomly packed beds are quite complex.[30] However, at very low values of Pe_m, dispersion is determined solely by molecular diffusion, wherein $D_L = D_T = D_m/\tau$ (see Figures 10 and 11 at $Pe_m < 0.4$). Note that the range of Pe_m is extended up to $Pe_m = 100$ in Figures 10 and 11 to investigate the tendency at higher Pe_m than 10. As seen the numerical results still fits to experimental data indicating that Taylor and boundary layer dispersions are still of minor concern at $Pe_m = 100$.

In this article, the porosity was varied from 0.365 for dense packing to 0.45 for loose packing, which is the typical observed value of porosity for random monosized spheres.[60,61] As previously mentioned in this article, the tortuosity decreases with increased porosity.[54] The obtained tortuosity factors for randomly monosized particles were in the range of 1.38–1.49, which is in agreement for normally observed values for packing of spheres (for an overview, see Lanfrey et al.[54]) Moreover, the obtained values of τ in this article are in agreement with the suggested value of $\tau = 1.4$ for spheres by Gunn.[62]

Comparisons of derived D_L and D_T in 3-D to 2-D packed-bed model

Relating the 3-D packed-bed model to its 2-D counterpart, the flow obviously has an extradimension to use, which makes the flow smoother. In the 2-D case, there is no flow through closely packed cylinders and the flow must go around such constrictions. This may increase the irregularities within the flow field and thus amplify the dispersion. Comparing the derived D_L and D_T from this 3-D packed-bed model to the previous 2-D models[26,32] yields that at very low Pe_m (molecular diffusion regime), both the 2-D and the 3-D approach correctly predict $D_L = D_T = D_m/\tau$. At higher Pe_m, when the dispersion due to convection is more important, the resulted D_L and D_T in a randomly packed 2-D system can be higher than the 3-D system.[32] However, this is obviously related to the 2-D porous-medium model that is used to simulate the dispersion. For instance, in the case of the 2-D periodic porous-medium model used in Edwards et al.,[26] at $Pe_m > 1$ the D_L is higher than the present study, whereas the D_T is much lower. This is, as pointed out in Edwards et al.,[26] related to the unit cell approach that was used in their study to derive D_T, which gives less intercellular lateral fluid motion, and, thus, lower D_T. Nevertheless, there are several applications where the flow can be considered to be 2-D, and, thus, a 2-D system is required to derive dispersion coefficients.

Conclusions

The methodology presented in this article has proven to be an effective tool that is easy to implement and can be used as an experiment instead of tracer dispersion in 3-D packed beds of spheres. Random and regular packing of spheres were generated applying appropriate numerical methods. Voronoi diagrams were used to divide the system of spheres into cells that each contains one particle. The local flow fields inside the Delaunay tetrahedrons were treated using Laurent series. After that, the whole flow pattern was obtained by minimization of the dissipation rate of energy for the dual stream function. As a result, a discretized 3-D packed-bed model was obtained with the known flow field, which makes it possible to extract the D_L and D_T for Peclet numbers (i.e., Pe_m) in the laminar flow regime. A summary of the major findings is as follows:

- The Thompson algorithm was found to be an effective means of handling the periodic boundary conditions for the Delaunay tessellation.
- The Laurent series for treating the local flow field as well as the dual stream function approach to approximate the flow make it possible to apply the variation method to obtain the overall flow. This methodology is shown to be successful for modeling the flow in 3-D packed beds.

- The tortuosity factor, τ, was found to decrease as a function of increasing porosity. Therefore, for identical systems, as the porosity decreases the tortuosity factor increases, which in turn decreases the D_L and D_T at very low Pe_m. Nevertheless, the effect of porosity at high Pe_m was insignificant.
- Changing the pore structure from random to perturbed hexagonal close-packed packing decreased the tortuosity factor. Therefore, a perturbed hexagonal close-packed packing system shows higher values of D_L and D_T at low Pe_m. However, at higher Pe_m ($Pe_m > 2$) because of lower irregularity of the flow front in the case of an ordered structure, the resulting D_L and D_T are lower compared to the system that had been packed randomly.
- The derived values of D_L and D_T in the 3-D packed beds of spheres are in good agreement with previous experimental data at low Pe_m. Therefore, the present approach to investigate dispersion in the laminar flow regime and effects of different packing parameters on dispersion can be considered to be acceptable.
- The use of dual stream function enables effective flow visualization in porous media.

Acknowledgment

The financial support of the Swedish Research Council and Formas is gratefully acknowledged.

Literature Cited

1. Herrmann I, Jourak A, Lundström TS, Hedström A, Viklander M. Phosphorus binding to Filtra P in batch tests. *Environ Technol*. 2012;33(9):1013–1019.
2. Herrmann I, Jourak A, Hedström A, Lundström TS, Viklander M. The effect of hydraulic loading rate and influent source on the binding capacity of phosphorus filters. *PLoS ONE*. 2013;8(8):e69017.
3. Amarasinghe BMWPK, Williams RA. Tea waste as a low cost adsorbent for the removal of Cu and Pb from wastewater. *Chem Eng J*. 2007;132(1–3):299–309.
4. Herrmann I, Jourak A, Gustafsson JP, Hedström A, Lundström TS, Viklander M. Modeling phosphate transport and removal in a compact bed filled with a mineral-based sorbent for domestic wastewater treatment. *J Contam Hydrol*. 2013;154:70–77.
5. Nijemeisland M, Dixon AG. CFD study of fluid flow and wall heat transfer in a fixed bed of spheres. *AIChE J*. 2004;50(5):906–921.
6. Yu B, Lee LJ, Cao H. Fractal characters of pore microstructures of textile fabrics. *Fractals*. 2001;9(2):155–163.
7. Movva S, Gang Z, Guerra D, Lee LJ. Effect of carbon nanofibers on mold filling in a vacuum assisted resin transfer molding system. *J Compos Mater*. 2009;43(6):611–620.
8. Nordlund M, Lundström TS, Frishfelds V, Jakovics A. Permeability network model for non-crimp fabrics. *Compos A*. 2006;37(6):826–835.
9. Nordlund M, Fernberg SP, Lundström TS. Particle deposition mechanisms during processing of advanced composite materials. *Compos A*. 2007;38(10):2182–2193.
10. Nordlund M, Lundström TS. Effect of multi-scale porosity in local permeability modelling of non-crimp fabrics. *Transp Porous Media*. 2008;73(1):109–124.
11. Masoodi R, Pillai KM. Darcy's law-based model for wicking in paper-like swelling porous media. *AIChE J*. 2010;56(9):2257–2267.
12. Masoodi R, Tan H, Pillai KM. Darcy's law-based numerical simulation for modeling 3D liquid absorption into porous wicks. *AIChE J*. 2011;57(5):1132–1143.
13. Lundström TS, Gustavsson LH, Jēkabsons N, Jakovics A. Wetting dynamics in multiscale porous media. Porous pore-doublet model, experiment and theory. *AIChE J*. 2008;54(2):372–380.
14. Frishfelds V, Lundström TS, Jakovics A. Lattice gas analysis of liquid front in non-crimp fabrics. *Transp Porous Media*. 2010;84(1):75–93.
15. Magnico P. Hydrodynamic and transport properties of packed beds in small tube-to-sphere diameter ratio: pore scale simulation using an eulerian and a lagrangian approach. *Chem Eng Sci*. 2003;58(22):5005–5024.
16. Dixon AG, Nijemeisland M. CFD as a design tool for fixed-bed reactors. *Ind Eng Chem Res*. 2001;40(23):5246–5254.
17. Succi S. The Lattice Boltzmann Equation: For Fluid Dynamics and Beyond. Oxford: Clarendon Press, 2001.
18. Chen S, Doolen GD. Lattice boltzmann method for fluid flows. *Annu Rev Fluid Mech*. 2003;30(1):329–364.
19. Manz B, Gladden LF, Warren PB. Flow and dispersion in porous media: lattice-boltzmann and NMR studies. *AIChE J*. 1999;45(9):1845–1854.
20. Freund H, Bauer J, Zeiser T, Emig G. Detailed simulation of transport processes in fixed-beds. *Ind Eng Chem Res*. 2005;44(16):6423–6434.
21. Brady JF, Sierou A. Accelerated stokesian dynamics simulations. *J Fluid Mech*. 2001;448:115–146.
22. Gunjal PR, Ranade VV, Chaudhari RV. Computational study of a single-phase flow in packed beds of spheres. *AIChE J*. 2005;51(2):365–378.
23. McKenna TF, Spitz R, Cokljat D. Heat transfer from catalysts with computational fluid dynamics. *AIChE J*. 1999;45(11):2392–2410.
24. Dixon AG, Nijemeisland M, Stitt EH. Systematic mesh development for 3D CFD simulation of fixed beds: contact points study. *Comput Chem Eng*. 2013;48:135–153.
25. Eppinger T, Seidler K, Kraume M. DEM-CFD simulations of fixed bed reactors with small tube to particle diameter ratios. *Chem Eng J*. 2011;166(1):324–331.
26. Edwards DA, Shapiro M, Brenner H, Shapira M. Dispersion of inert solutes in spatially periodic, two-dimensional model porous media. *Transp Porous Media*. 1991;6(4):337–358.
27. Hellström JGI, Frishfelds V, Lundström TS. Mechanisms of flow-induced deformation of porous media. *J Fluid Mech*. 2010;664:220–237.
28. Berlyand L, Panchenko A. Strong and weak blow-up of the viscous dissipation rates for concentrated suspensions. *J Fluid Mech*. 2007;578:1–34.
29. Li Z, Mallinson G. Dual stream function visualization of flows fields dependent on two variables. *Comput Vis Sci*. 2006;9(1):33–41.
30. Koch DL, Brady JF. Dispersion in fixed beds. *J Fluid Mech*. 1985;154:399–427.
31. Koch DL, Cox RG, Brenner H, Brady JF. The effect of order on dispersion in porous media. *J Fluid Mech*. 1989;200:173–188.
32. Jourak A, Frishfelds V, Lundström TS, Herrmann I, Hedström A. The calculations of dispersion coefficients inside two-dimensional randomly packed beds of circular particles. *AIChE J*. 2013;59(3):1002–1011.
33. Jourak A, Frishfelds V, Hellström JGI, Lundström TS, Herrmann I, Hedström A. Longitudinal dispersion coefficient: effects of particle-size distribution. *Transp Porous Media*. 2013;99(1):1–16.
34. Ljung A, Frishfelds V, Lundström TS, Marjavaara BD. Discrete and continuous modeling of heat and mass transport in drying of a bed of iron ore pellets. *Drying Technol*. 2012;30(7):760–773.
35. Frishfelds V, Lundström TS. Modelling of particle deposition during impregnation of dual scale fabrics. *Plast Rubber Compos*. 2011;40:65–69.
36. Frishfelds V, Hellström JGI, Lundström TS, Mattsson H. Fluid flow induced internal erosion within porous media: modelling of the no erosion filter test experiment. *Transp Porous Media*. 2011;89:1–17.
37. Zhang W, Thompson KE, Reed AH, Beenken L. Relationship between packing structure and porosity in fixed beds of equilateral cylindrical particles. *Chem EngSci*. 2006;61(24):8060–8074.
38. Song C, Wang P, Makse HA. A phase diagram for jammed matter. *Nature*. 2008;453(7195):629–632.
39. Maier RS, Kroll DM, Bernard RS, Howington SE, Peters JF, Davis HT. Hydrodynamic dispersion in confined packed beds. *Phys Fluids*. 2003;15:3795–3815.
40. Frishfelds V, Lundström TS, Jakovics A. Permeability of clustered fiber networks: modeling of the unit cell. *Mech Compos Mater*. 2003;39(3):265–272.
41. Jodrey W, Tory E. Computer-simulation of close random packing of equal spheres. *Phys Rev A*. 1985;32(4):2347–2351.
42. Anikeenko A, Gavrilova M, Medvedev N. Shapes of delaunay simplexes and structural analysis of hard sphere packings. In: Generalized Voronoi Diagram: A Geometry-Based Approach to Computational Intelligence. Heidelberg, Germany: Springer 2009:13–45.
43. Skoge M, Donev A, Stillinger FH, Torquato S. Packing hyperspheres in high-dimensional euclidean spaces. *Phys Rev E*. 2006;74(4):041127.
44. Chen X, Papathanasiou TD. The transverse permeability of disordered fiber arrays: a statistical correlation in terms of the mean nearest interfiber spacing. *Transp Porous Media*. 2008;71(2):233–251.

45. Thompson KE. Fast and robust delaunay tessellation in periodic domains. *Int J Numer Methods Eng*. 2002;55(11):1345–1366.
46. Shewchuk J. PhD Thesis. Pennsylvania: School of Computer Science, Carnegie Mellon University, 1997.
47. Drummond J, Tahir M. Laminar viscous flow through regular arrays of parallel solid cylinders. *Int J Multiphase Flow*. 1984;10(5):515–540.
48. van Genuchten MTH, Alves WJ. Analytical solutions of the one-dimensional convective-dispersive solute transport equation. In: Technical Bulletin, vol. 1661, Washington, DC: U.S. Department of Agriculture, 1982:79–80.
49. Coelho MAN, Guedes de Carvalho JRF. Transverse dispersion in granular beds. Part 1. Mass transfer from a wall and the dispersion coefficient in packed beds. *Chem Eng Res Des*. 1988;66(2):165–177.
50. Bear J. Dynamics of Fluids in Porous Media. New York: American Elsevier,1972.
51. Han NW, Bhakta J, Carbonell RG. Longitudinal and lateral dispersion in packed beds: effect of column length and particle size distribution. *AIChE J*. 1985;31(2):277–288.
52. van Genuchten MTH. Determining Transport Parameters from Solute Displacement Experiments, vol. 118. Riverside, CA: Salinity Laboratory, 1980.
53. Šimůnek J, van Genuchten MT, Šejna M, Toride N, Leij FJ. The STANMOD Computer Software for Evaluating Solute Transport in Porous Media Using Analytical Solutions of Convection-Dispersion Equation, Versions 1 0 and 2 0, IGWMC-TPS-71. Golden, Colorado: International Ground Water Modeling Center, Colorado School of Mines,1999:32.
54. Lanfrey PY, Kuzeljevic ZV, Dudukovic MP. Tortuosity model for fixed beds randomly packed with identical particles. *Chem Eng Sci*. 2010;65(5):1891–1896.
55. Hassinger R, von Rosenberg D. A mathematical and experimental examination of transverse dispersion coefficients. *Soc Pet Eng J*. 1968;8(2):195–204.
56. Blackwell RJ. Laboratory studies of microscopic dispersion phenomena. *Soc Pet Eng J*. 1962;2(1):1–8.
57. Edwards MF, Richardson JF. Gas dispersion in packed beds. *Chem Eng Sci*. 1968;23(2):109–123.
58. Blackwell R, Rayne J, Terry WM. Factors influencing the efficiency of miscible displacement. *Trans AIME*. 1959;216(1):1–9.
59. Gunn DJ, Pryce C. Dispersion in packed beds. *Trans Inst Chem Eng*. 1969;47:341–350.
60. Onoda GY, Liniger EG. Random loose packings of uniform spheres and the dilatancy onset. *Phys Rev Lett*. 1990;64(22):2727–2730.
61. Mota M, Teixeira J, Bowen WR, Yelshin A. Binary spherical particle mixed beds: porosity and permeability relationship measurement. *Trans Filtr Soc*. 2001;17:101–106.
62. Gunn DJ. Axial and radial dispersion in fixed beds. *Chem Eng Sci*. 1987;42(2):363–373.

Appendix A : Minimization of Dissipation Rate of Energy

Let us prove that the following functional is minimal for Stokesian flow in the system with periodic boundary conditions and either nonslip or free slip conditions on particles

$$\Phi[\boldsymbol{\psi}]=\iiint_V \frac{\boldsymbol{\omega}^2}{2}dV \tag{A1}$$

where $\boldsymbol{\psi}=\boldsymbol{\psi}(x, y, z)$ is the stream function vector dependent on spatial position and $\boldsymbol{\omega}=\nabla\times\mathbf{u}=\nabla\times(\nabla\times\boldsymbol{\psi})$ is the vorticity vector. It is assumed that the stream function within each particle is a constant vector. Suppose that minimal value of the functional is achieved at the distribution of the stream function $\boldsymbol{\psi}_0=\boldsymbol{\psi}_0(x, y, z)$. The vorticity corresponding to this stream function is $\boldsymbol{\omega}_0$. Let us add an infinitesimal perturbation to that stream function

$$\boldsymbol{\psi}=\boldsymbol{\psi}_0+\delta\boldsymbol{\psi} \tag{A2}$$

The functional at the perturbed value neglecting higher order variations with respect to $\delta\boldsymbol{\psi}$ is

$$\Phi[\boldsymbol{\psi}]=\Phi[\boldsymbol{\psi}_0]+\iiint_V(\nabla\times(\nabla\times\boldsymbol{\psi}_0))\cdot(\nabla\times(\nabla\times\delta\boldsymbol{\psi}))dV=\Phi[\boldsymbol{\psi}_0]+\iiint_V\boldsymbol{\omega}_0\cdot(\nabla\times(\nabla\times\delta\boldsymbol{\psi}))dV \tag{A3}$$

The extremum value of functional at $\boldsymbol{\psi}_0$ is proven if the second term in the right hand side is zero at any infinitesimal perturbation that satisfies the boundary conditions. Using the identity of vector calculus

$$\nabla(\mathbf{A}\times\mathbf{B})=\mathbf{B}\cdot(\nabla\times\mathbf{A})-\mathbf{A}\cdot(\nabla\times\mathbf{B}) \tag{A4}$$

we can integrate the second term by parts and apply the divergence theorem

$$\begin{aligned}\iiint_V\boldsymbol{\omega}_0\cdot(\nabla\times(\nabla\times\delta\boldsymbol{\psi}))dV&=-\iiint_V\nabla(\boldsymbol{\omega}_0\times(\nabla\times\delta\boldsymbol{\psi}))dV+\iiint_V(\nabla\times\boldsymbol{\omega}_0)\cdot(\nabla\times\delta\boldsymbol{\psi})dV\\&=-\iint_S(\boldsymbol{\omega}_0\times\delta\mathbf{u})d\mathbf{S}+\iiint_V(\nabla\times\boldsymbol{\omega}_0)\cdot(\nabla\times\delta\boldsymbol{\psi})dV\end{aligned} \tag{A5}$$

The first term in the right hand side vanishes due to nonslip boundary conditions at solid surfaces $\delta\mathbf{u}=0$and periodic boundary conditions at the walls. It cancels also for free surface flows like bubbles, where $\boldsymbol{\omega}_0=0$ at the surface. Doing the same procedure once more yields

$$\begin{aligned}\iiint_V(\nabla\times\boldsymbol{\omega}_0)\cdot(\nabla\times\delta\boldsymbol{\psi})dV&=-\iiint_V\nabla(\nabla\times\boldsymbol{\omega}_0)\times\delta\boldsymbol{\psi})dV+\iiint_V(\nabla\times(\nabla\times\boldsymbol{\omega}_0))\cdot\delta\boldsymbol{\psi}dV\\&=-\iint_S(\nabla\times\boldsymbol{\omega}_0)\times\delta\boldsymbol{\psi})d\mathbf{S}+\iiint_V(\nabla\times(\nabla\times\boldsymbol{\omega}_0))\cdot\delta\boldsymbol{\psi}dV\end{aligned} \tag{A6}$$

The first term cancels for periodic boundaries if the total flow rate is fixed. As the stream function vector is constant and fixed within particles then $\delta\boldsymbol{\psi}=0$ at the surface of particles and the first term cancels, too. The second term cancels for Stokesian flow: $\nabla\times(\nabla\times\boldsymbol{\omega}_0)=\mathbf{0}$. It is clear that functional tends to be minimal globally for fixed flow rate through the system giving the stream function values for all the particles except one, where it can be set freely. Also, note that an additional constraint (e.g., $\nabla\boldsymbol{\psi}=0$) is required to get one and only one solution for the global stream function at given periodic boundary conditions. Thus, minimization of functional with respect to the stream function vector is acceptable.

Appendix B: Permeability

A fluid can only generate tangential viscous stresses on a solid surface with a nonslip boundary condition. Thus, to calculate the drag force on the particle, the vorticity close to it must be known. The viscous force exerted on the particle is an integral of vorticity $\boldsymbol{\omega}^{\mathrm{sph}}$ at the surface

$$f_{\text{viscous}} = \mu \iint_{\text{sph}} \boldsymbol{\omega}^{\text{sph}} \times \mathbf{n} \mathrm{dS} \tag{B1}$$

where **n** is the normal direction related to the particle surface, and index sph denotes the sphere. Then, normal force, in turn, depends on the pressure P distribution around the particle. The force, for example, in the z-direction is

$$f_{z,\text{normal}} = \iint_{\text{sph}} P n_z \mathrm{dS} = R^2 \int_0^{2\pi} \int_0^{\pi} P(\theta, \phi) sin(\theta) cos(\theta) d\theta d\phi$$

$$= -\frac{R^2}{2} \int_0^{2\pi} \int_0^{\pi} \frac{\partial P}{\partial \theta} sin^2 \theta d\, \theta d\phi \tag{B2}$$

where axis $\theta = 0$ coincides with z axis, and inner integral has been integrated by parts.

According to the momentum equation, the change of pressure at the surface of the particle is

$$\frac{1}{R} \frac{\partial P}{\partial \theta} = \mu \frac{\partial \omega_\phi^{\text{sph}}}{\partial n} \tag{B3}$$

where n is coordinate in normal direction from the surface of particle. Combining viscous and normal forces results in the following force on the particle

$$f_z = \mu R^2 \int_0^{2\pi} \int_0^{\pi} \left(\omega_\phi^{\text{sph}} - \frac{R}{2} \frac{\partial \omega_\phi^{\text{sph}}}{\partial n} \right) sin^2 \theta d\theta d\phi \tag{B4}$$

Thus, the normal force dominates in highly packed systems. The sum of all drag forces on the particles should be equal to the driving pressure difference, as the system with periodic boundary conditions has no walls. Hence, Darcy's law can be rewritten as follows

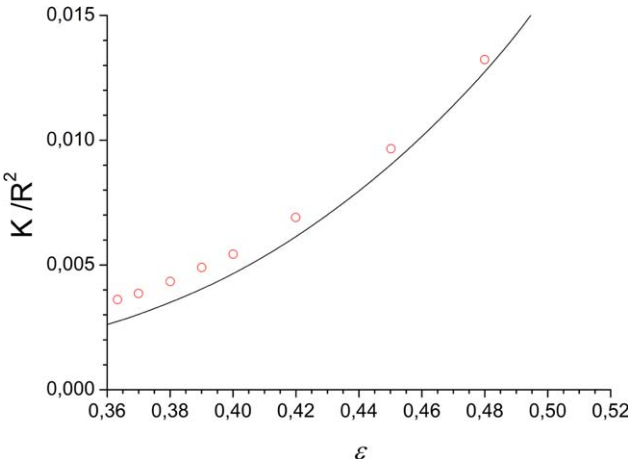

Figure B1. Symbols (o) show calculated permeability vs. porosity.

Line represents Rumpf and Gupte's formula for packed bed of spheres: $\frac{K}{R^2} = \frac{\varepsilon^{5.5}}{1.4}$; R is radius of a sphere. [Color figure can be viewed in the online issue, which is available at wileyonlinelibrary.com.]

$$\langle \mathbf{v} \rangle = \frac{\mathbf{K}}{\mu} \frac{\sum_i \mathbf{f}_i}{V}, \tag{B5}$$

where i is the sum over all particles, V is the volume of the system, and $\langle \mathbf{v} \rangle$ denotes the average velocity of the system. The permeability tensor **K** can be obtained from this relationship. Figure B1 shows the relationship between the obtained permeabilities and porosities in the packed-bed model that are compared to Rumpf and Gupte's formula for packed bed of spheres.

Manuscript received Nov. 30, 2012, and revision received Sept. 29, 2013.